ACS OMEGA

Open Access

http://pubs.acs.org/journal/acsodf

Article

Catalytic Activity of Nonaggregating Cu Nanoparticles Supported in Pores of Zeolite for Aerobic Oxidation of Benzyl Alcohol

Shunya Sakane, Kai Akimoto, Kishin Konishi, Kenta Takaoka, Harunobu Iwatsuki, Mayu Akutsu, Toshiki Sugai, and Hideki Tanaka*

Cite This: *ACS Omega* 2024, 9, 970−976

Read Online

ACCESS | Metrics & More | Article Recommendations | Supporting Information

ABSTRACT: Cu nanoparticles (NPs) as catalysts have the good advantage of being more abundant than noble metal NPs. In this study, we synthesized nonaggregating Cu NPs supported in Y-type zeolite by the photoreduction method. In this method, Cu ions in pores of zeolite can be slowly reduced with a small amount of reductant at room temperature. The high-resolution transmission electron microscope, energy dispersive X-ray spectroscopy, X-ray diffraction patterns, and UV−Vis spectra supported that nonaggregating Cu NPs existed in the pores of zeolite. Catalytic activities of Cu NP-zeolite were investigated for the aerobic oxidation of benzyl alcohol. Our Cu NP-zeolite had a large turnover frequency of 17 h^{-1}. The yield of benzaldehyde increased in proportion to the amount of Cu loading at ≤0.5 wt %, indicating that Cu NPs in pores of zeolite work as catalysts for selective aerobic oxidation of benzyl alcohol. The high catalytic activity was brought by nonaggregating Cu NPs in pores of zeolite. The catalytic reaction for other aromatic alcohols with electron-donating groups proceeded, whereas it did not proceed for the aromatic alcohols with electron-withdrawing groups or aliphatic alcohols, indicating that the interaction between zeolite and the benzene ring also contributed to the reaction. This study would be expected to contribute to the development of Cu NP catalysts.

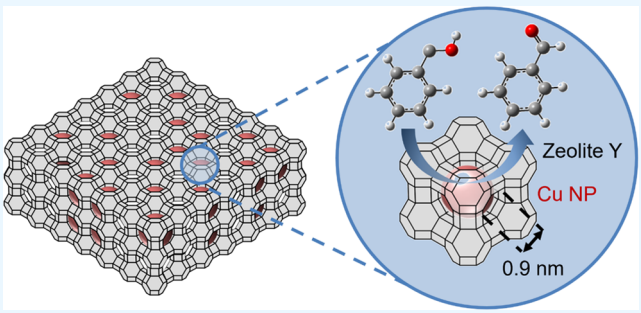

INTRODUCTION

Metal nanoparticles (NPs) are expected to exhibit high catalytic activity due to their large surface area.[1−17] While noble metal NPs such as Au or Pt have been usually studied as catalysts,[18−22] Cu NPs as catalysts have a good advantage of being more abundant than these noble metal NPs.[23] Cu NPs have been applied to catalytic activity for various chemical reactions, such as hydrogen evolution reaction, reduction of CO_2 to liquid fuels, and water−gas shift reaction.[23] However, it is difficult to synthesize Cu NPs due to the higher ionized tendency of Cu^{2+} ions than that of noble metal ions, and Cu NPs thus synthesized are also easily oxidized upon exposure to air. Therefore, it is difficult to synthesize highly catalytically active Cu NPs, namely, metallic Cu NPs without oxide. Moreover, for higher catalytic activity, it is more difficult to synthesize smaller Cu NPs, preferably 1 nm or less in diameter.

Zeolite has attracted attention as a synthesis-supporting material of small NPs due to its small pores (<1 nm), in which NPs can be prevented from aggregating and oxidizing in the pores. There have also been many reports about Cu ions supported in pores of zeolite.[24−27] However, the supported Cu ions easily migrate and tend to form aggregates not only inside but also on the surface of the zeolite during the reduction to Cu^0.[28] For instance, when Cu ions supported in pores of zeolite were reduced by hydrogen at high temperature (460 °C), synthesized Cu NPs larger than the pore size of zeolite were observed.[29,30] In the case of sodium borohydride used as a reductant, aggregated Cu NPs were reported to form on the surface of zeolite due to rapid reduction.[28] Hydrazine as a reductant under slow reduction conditions realized the dominant formation of Cu NPs in pores of zeolite.[28] Therefore, slow reduction may be the key to synthesis in pores of zeolite. To this end, the photoreduction method for Cu ions can be expected to be a promising candidate because the photoreduction tends to be slow.[31]

In this study, we synthesized nonaggregating Cu NPs in pores of zeolite by the combination of ion-exchange and photoreduction methods.[24,31−37] Y-type zeolite, which has a relatively large pore size of ∼0.9 nm, was used because the size of acetate ions as the trigger of photoreduction by n-π^* transition[38] is smaller than the pore size of Y-type zeolite.[39] We also investigated their catalytic activity for the aerobic oxidation of benzyl alcohol. There have been several studies

Received: September 18, 2023
Revised: December 13, 2023
Accepted: December 18, 2023
Published: December 28, 2023

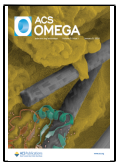

about catalysts for benzyl alcohol oxidation using noble metal NPs with zeolite, such as Au NP-zeolite, and PdO/CuO NP-zeolite.[9,40] We herein report that the nonaggregating Cu NPs in pores of zeolite exhibited high catalytic activity for selective aerobic oxidation of benzyl alcohol to benzaldehyde even in the above mild condition (Figure 1a).

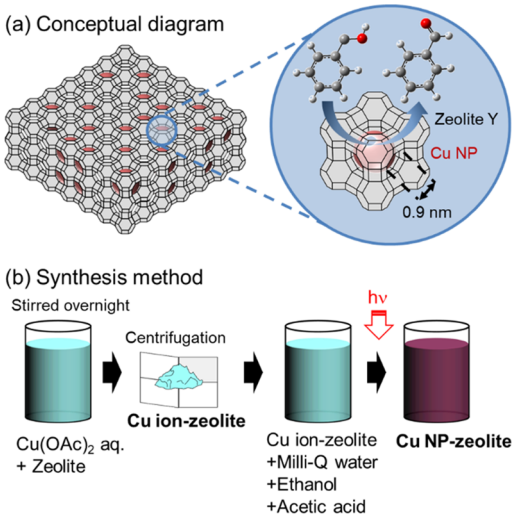

Figure 1. (a) Conceptual diagram of the catalytic activity of Cu NP-zeolite for benzyl alcohol oxidation. (b) Illustration of the synthesis method of Cu NP-zeolite.

EXPERIMENTAL SECTION

Material Synthesis. Y-type zeolite (1 g, TOSOH, HSZ-320HOA), which has 0.9 nm pore and 1.2 nm supercage, was dissolved in 50 mL of 1.6 mM copper acetate monohydrate ($Cu(OAc)_2 \cdot H_2O$) solution and stirred overnight, forming Cu ion-zeolite dispersion.[41] Cu ion-zeolite precipitates were separated from the solution by centrifugal separation. After the precipitates were rinsed with Milli-Q water (18.2 MΩ cm^{-1}), they were dried in an oven at 120 °C, forming Cu ion-zeolite powders. The obtained powders were dissolved in a mixture of 45 mL of Milli-Q water, 5 mL of ethanol, and 1.35 μL of acetic acid and thereafter stirred with ultrasonication (HONDA W-113:45 kHz, 5 min). The mixed solution was irradiated with a Hg lamp (Hamamatsu Photonics: L9588−01A) of 15 mW cm^{-2} at 254 nm for 24 h with stirring, forming Cu NP-zeolite by photoreduction. These synthesis methods are illustrated in Figure 1b. Since the mass concentration of Cu $(OAc)_2 \cdot H_2O$ in this case corresponds to 0.5 wt %, the obtained Cu NP-zeolite is abbreviated as CuY0.5 in this paper.

Characterization. The dispersion of Cu NP-zeolite (3 mL) in quartz cells was characterized by diffuse reflectance (DR) UV−Vis spectrometry with a UV−Vis−NIR spectrometer (Shimadzu, UV-3600). The DR UV−Vis spectra were calculated by Kubelka−Munk function $F(R)$ to convert diffuse reflectance into an equivalent absorption coefficient as follows

$$F(R) = \frac{(1-R)^2}{2R} \quad (1)$$

where R is the reflectance. The Cu NP-zeolite powders obtained by drying in a vacuum were characterized by powder X-ray diffraction (XRD) with an X-ray diffractometer (Rigaku, SmartLab) with Cu Kα radiation (0.154 nm) under operation at 40 kV and 40 mA. The structures of the powders were observed by scanning electron microscopy (SEM) and energy dispersive X-ray spectroscopy (EDX) with a field-emission SEM (Hitachi High-Technologies, S-5500), and high-resolution transmission electron microscopy (HRTEM) with a TEM (Thermo Fisher Scientific, Tecnai G2 F20 S-TWIN, FEI).

Evaluation of Catalytic Activity for Aerobic Oxidation of Benzyl Alcohol. Cu NP-zeolite powder (20 mg), tridecane (50 μL), benzyl alcohol (2 mmol), and K_2CO_3 (10 mmol) (dehydrating agent) were added to acetonitrile (10 mL). The solution was reacted with stirring at 700 rpm by a synthesizer (EYELA, Chemi Station, pps-2510) at 60 °C under air. The reaction temperature was determined concerning ref 40. The catalyst was extracted from the reacted solution by centrifugal separation. We confirmed that the extracted solution did not contain the catalyst (Cu NP-zeolite) by the leaching test, which is described in the Supporting Information. The reacted solution was evaluated by gas chromatography (GC) (Shimadzu, GC-2014). In GC, tridecane was used as an internal standard to prepare a calibration curve for quantification. The amounts of benzyl alcohol and benzaldehyde were determined by the calibration curve.

RESULTS AND DISCUSSION

Figure 2a shows the XRD patterns of Cu NP-zeolite. Intensities of the peaks at 43.31 and 50.41 increased as the

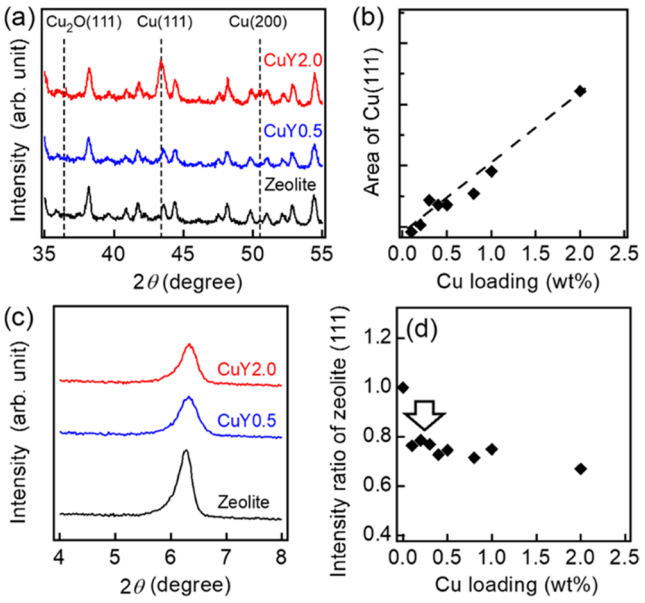

Figure 2. (a) XRD patterns of Y-type zeolite and CuY0.5 and CuY2.0. (b) Area of Cu(111) peak, which was calculated by using normalized patterns with intensity of zeolite (331) at 15.8°. (c) Enlarged XRD patterns around zeolite (111) (~6.3°) of Y-type zeolite and CuY0.5 and CuY2.0. (d) XRD intensity ratio of zeolite (111) as a function of Cu loading amounts.

Cu loading increased while those of other peaks observed in zeolite (black line) did not change. According to JCPDS file no. 4-0836, the peaks at 43.31 and 50.41 were found to correspond to the (111) and (200) crystal planes of the fcc phase of Cu, respectively, and other peaks observed in zeolite were assignable to crystal planes of zeolite. No peaks originating from Cu_2O at 36.41° or CuO at 35.51° were

https://doi.org/10.1021/acsomega.3c07156
ACS Omega 2024, 9, 970−976

observed (JCPDS files 5-0667 and 48-1548). This suggests that the loading Cu was converted to metallic Cu in zeolite. Considering that the amount of zeolite was constant in all samples, the relative amount of copper can be estimated by normalizing the peak intensity of Cu (111) with the peak intensity of zeolite (331) (~15.8°) (Figure S1) and subtracting the XRD pattern of only zeolite. As shown in Figure 2b, the relative Cu amount thus estimated is proportional to the amount of Cu loading. These indicate that all the loading Cu was converted to metallic Cu in zeolite without dissipation. 2θ values of the zeolite (111) peak were found to increase as Cu amounts increased, as shown in Figure 2c. The peak intensity ratio was also calculated by dividing zeolite (111) (~6.3°) intensity of zeolite without Cu NPs by that of Cu NP-zeolite, which is shown in Figure 2d. Peak intensity ratio of zeolite (111) was found to be reduced when Cu was loaded. This peak shift and peak intensity reduction are due to the deformation of lattice spacing of zeolite (111), which supports the idea that Cu NPs were formed in the pores of zeolite.

Figure 3a,b shows the SEM-EDX images of CuY0.5. In the SEM image (Figure 3a), grains of 500 nm were observed. Since

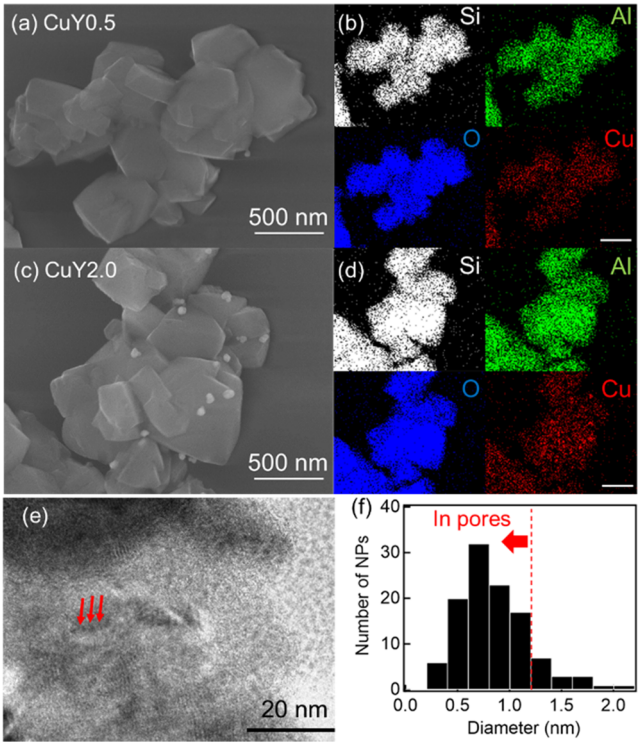

Figure 3. (a) SEM and (b) elemental mapping images of Si, Al, O, and Cu of CuY0.5. (c) SEM and (d) elemental mapping images of Si, Al, O, and Cu of CuY2.0. In panels (b) and (d), the scale bar represents 500 nm. (e) TEM image of CuY0.5, where arrows indicate NP. (f) Histogram showing the particle size distribution (N = 113).

similar grains were also observed in zeolite without Cu NPs (Figure S2), the grains are zeolite. The EDX of the grain showed the existence of not only Si, Al, and O coming from Y-type zeolite but also Cu. Considering that Cu ions were introduced into pores of zeolite and were reduced to Cu^0, this result suggests that the Cu NPs exist in pores of zeolite although no apparent Cu NPs were observed in the SEM image probably due to lack of resolution. Another group also previously reported that Cu was observed by TEM-EDX mapping in a region without black nanoparticles when Cu NPs were formed in pores of SOD-zeolite.[42] Cu amounts in zeolite were estimated by quantitative analysis of EDX (Figure S3). The Cu amounts were well proportional to the Cu loading. Since this tendency promises Cu loading to zeolite even though no apparent Cu NPs were observed, the existence of Cu NPs in the pores of zeolite was also supported.

In contrast, large NPs (~44 nm) were observed in the SEM image for CuY2.0, as shown in Figure 3c. These NPs seem as if they are attached to the surface of the zeolite, not to the inside. In addition, these NPs were found to correspond well to the densely populated areas in the EDX images (Figure 3d). These results suggest that Cu NPs did not only exist in the pores of zeolite but also existed on the surface of zeolite in CuY2.0. Although the Cu loading amount was continuously increasing (Figure 2b), most of the large Cu NPs were detected at ≥0.8 wt %, indicating that Cu NPs in pores aggregated at ≥0.8 wt %. In other words, this result supports that nonaggregating Cu NPs were formed in pores for 0.5 wt % or less-Cu-containing zeolite.

Figure 3e shows the HRTEM image of CuY0.5. The observed lattice image was assigned to that of zeolite, which supports the idea that the grains observed by SEM were zeolite. In this HRTEM image, some small NPs, including those indicated by the arrows, were also observed. The diameter histogram of these NPs is shown in Figure 3f. The average diameter was estimated to be 0.85 nm, and more than 88% of NPs were distributed less than 1.2 nm. Considering that the supercage size of Y-type zeolite was 1.2 nm, these NPs correspond to Cu NPs formed in the pores of zeolite.

DR UV−Vis spectra are shown in Figure 4a. The peak at 567 nm that appeared in CuY2.0 was ascribed to the LSPR of the Cu NPs. On the other hand, the peak at 580 nm that appeared in CuY0.5 was shifted to a longer wavelength compared to the LSPR of Cu NPs. This red shift was consistent with Cu NPs existing in pores of zeolite.[28] Here, we calculated the absorption cross-section of Cu NPs on the surface of zeolite and Cu NPs in the pores of zeolite, as shown in Figure S4. The details of this calculation are described in the Supporting Information. Figure S4 shows that the LSPR peak of Cu NPs in the pores of zeolite is red-shifted compared with the Cu NPs on the surface of zeolite. Namely, the above red shift of LSPR supported that Cu NPs were formed in pores of zeolite for CuY0.5, while Cu NPs were also formed on the surface of zeolite for CuY2.0. These results are consistent with the SEM-EDX results. The peak wavelength of LSPR was almost constant for 0.5 wt % or less-Cu-containing zeolite, as shown in Figure 4b. Considering that in general, the LSPR peak wavelength depends on particle size or distance between particles, this constant LSPR peak position indicates that the size and distribution of Cu NPs were uniform and homogeneous, respectively. These also support the Cu NP formation in the pores of zeolite. For CuY0.5, LSPR peak intensities were obtained by subtracting the intensity of zeolite, as shown in Figure 4c. The peak intensity was found to be proportional to the Cu loading. This indicates that the number of Cu NPs in the pores of zeolite increased as the amount of Cu loading increased at ≤0.5 wt %.

The catalytic activity of Cu NP-zeolite was evaluated for the aerobic oxidation of benzyl alcohol. In gas chromatographic analysis, benzaldehyde was observed at the retention time of ~5.8 min only for zeolite with Cu NPs while acetonitrile as a solvent (~2.0 min), benzyl alcohol (~8.7 min), and tridecane

https://doi.org/10.1021/acsomega.3c07156
ACS Omega 2024, 9, 970−976

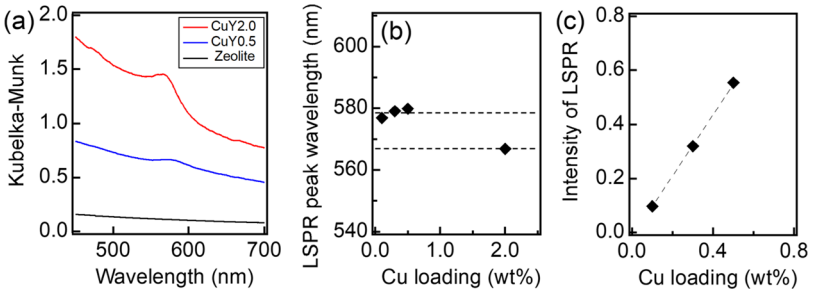

Figure 4. (a) DR UV−Vis spectra of the Y-type zeolite and CuY0.5 and CuY2.0. (b) LSPR peak wavelength as a function of Cu loading. (c) Intensity of LSPR of pore-loaded zeolite (0.1−0.5 wt %), which was obtained by subtracting the intensity of zeolite.

Table 1. Comparison of Catalytic Activity of Cu NPs for Oxidation of Benzyl Alcohol

reference	catalyst	NP size (nm)	oxidant	reaction temperature (°C)	TOF (h^{-1})
this study	CuY0.5	≤1.2	air	60	17
this study	CuY0.5	≤1.2	no (Ar)	60	2.9
this study	zeolite		air	60	0
44	Cu NPs/Cr_2O_3	2−5	air	120	16
	Cu NPs	not shown	air	120	0
45	Cu/CuO/cyclodextrin	30	air	140−150	0.0045
46	Cu NPs/cellulose	2−10	air	80	0.006
	Cu NPs/cellulose + microwave	2−10	air	80	13

as an internal standard (∼42 min) were observed both for zeolite with and without Cu NPs. On the other hand, the benzoic acid (∼10.5 min) was not observed for both. The selectivity was also calculated for benzyl alcohol oxidation to benzaldehyde. All samples exhibited high selectivity of more than 90% as shown in Table S1, namely, the amount of produced benzaldehyde is in good agreement with the amount of consumed benzyl alcohol. Therefore, the detection of benzaldehyde for zeolite with Cu NP suggests that benzyl alcohol was oxidized by Cu NP as a catalyst as follows

$$\text{benzy alcohol} \xrightarrow{\text{Cu NP-zeolite}} \text{benzaldehyde} \quad (2)$$

The catalytic activity was also investigated in an Ar atmosphere (without O_2) for 3 h. However, the catalytic reaction did not proceed as well as the reaction under air (Table 1), indicating that the catalytic reaction under air proceeded through O_2. The most probable process of this catalytic reaction can be explained as follows: Cu NPs abstract hydrogen from the α carbon adsorbed alkoxide and O_2 in air removes the hydrogen from the Cu NP surface.[43]

Figure 5a shows the reaction time dependence of the catalytic activity for CuY0.5. The yield of benzaldehyde monotonically increased until 24 h. At 24 h, 0.30 mmol of benzaldehyde was produced while 0.31 mmol of benzyl alcohol was reduced, which indicates selective oxidation of benzyl alcohol to benzaldehyde. Considering that the catalytic reaction is a first-order one, the reaction time (t) dependence of the amounts of benzaldehyde ($[\text{Aldehyde}]_t$) is expressed with the following equation using the reaction rate constant k

$$\ln\left(1-\frac{[\text{Aldehyde}]_t}{[\text{Alcohol}]_0}\right)=-kt \quad (3)$$

The ln (1-$[\text{Aldehyde}]_t/[\text{Alcohol}]_0$) values were plotted as a function of reaction time in the range of 0−12 h in Figure 5b. The linearly fitted line is in good agreement with the experimental data, indicating that the reaction is a first-order

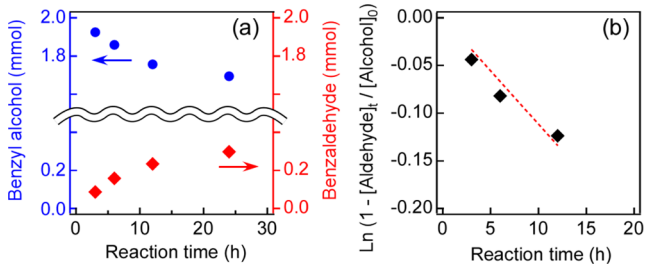

Figure 5. (a) Reaction time dependence of benzyl alcohol amounts (left) and benzaldehyde yield (right axis). In this reaction, CuY0.5 was used as a catalyst at 60 °C. (b) Reaction time dependence of Ln (1-$[\text{Aldehyde}]_t/[\text{Alcohol}]_0$). The dashed line in panel (b) indicates the linearly fitted one.

reaction in the range of 0−12 h. From the above eq 3, the reaction rate constant was obtained to be 0.011 h^{-1}. Here, to compare the catalytic activities with other reports, the benzaldehyde yield (mol) per Cu of 1 mol (turnover number; TON) and TON per reaction time (h) (turnover frequency; TOF) were calculated as the following equations

$$\text{TON} = \frac{\text{benzaldehyde yield (mol)}}{\text{Cu amounts in the catalyst (mol)}} \quad (4)$$

$$\text{TOF} = \frac{\text{TON}}{\text{reaction time (h)}} \quad (5)$$

Table 1 shows TOF of CuY0.5, zeolite, and Cu-related NPs previously reported.[44−46] CuY0.5 achieved a high TOF of 17 h^{-1} at 6 h in the air. This value was higher than those of any other reports where air was used as an oxidant despite the mild condition (lower reaction temperature than other reports). Considering that the NP size of CuY0.5 was the smallest among other reports, this high TOF was brought by the extremely small Cu NPs in the pores of zeolite.

To discuss this high catalytic activity, Cu loading (wt %) dependence of benzaldehyde yield was obtained for the

https://doi.org/10.1021/acsomega.3c07156
ACS Omega 2024, 9, 970−976

reaction of a sufficiently long time (24 h), as shown in Figure 6a. All Cu loading in this range forms Cu NPs in pores as

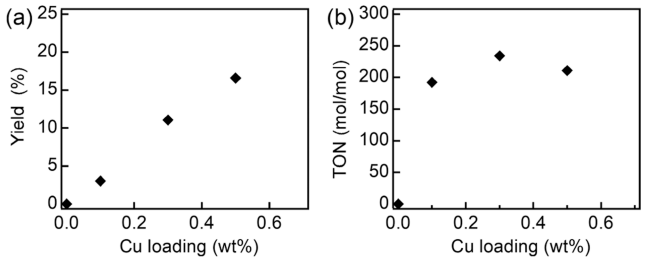

Figure 6. (a) Yield of benzaldehyde and (b) TON (mol/mol) as a function of Cu loading (wt %) for pore-loaded zeolite (≤0.5 wt %).

mentioned in SEM-EDX analysis. The yield was well proportional to the amount of Cu loading for this pore-loaded zeolite. This proportional tendency indicates that Cu NPs of ≤1.2 nm in pores of zeolite worked as catalysts. In other words, pores of zeolite helped the homogeneous formation of Cu NPs and inhibition of their aggregation spoiling their catalytic activity. In contrast, the yield seemed to be saturated, and the TON was reduced at more than 0.5 wt % Cu loading as shown in Figure S5. As a result, optimized Cu loading was 0.1−0.5 wt %. As noted in SEM-EDX analysis, large Cu NPs were observed outside of the pores in this range. Namely, these large Cu NPs were less effective for catalytic reaction than those inside the pores of zeolite. This result supports the effectiveness of nonaggregating Cu NPs in pores of zeolite for catalytic reaction, and active sites were Cu NPs in pores of zeolite. As shown by these results, the pore-loaded zeolite exhibited a high TON of almost 200 mol/mol, as shown in Figure 6b. This TON value corresponds to the produced benzaldehyde of more than 4 molecules per 1 Cu NP. This result indicates that one Cu NP in pores of zeolite can cyclically produce benzaldehyde more than 4 times. To investigate the stability of our catalyst, we performed SEM-EDX analysis after catalytic reaction. From the SEM image, there are no specific differences in the zeolite grain after reaction (Figure S6). We also confirmed that the Cu amounts in zeolite were maintained after catalytic reaction by quantitative analysis of EDX, indicating that this catalyst can be reused. In fact, we confirmed that the reaction proceeded even when we repeated the reaction 3 times. These results are detailed and are shown in the Supporting Information.

Here, we calculated the total surface area (S_{total}) of Cu NPs for all samples, where we hypothesized that (1) the size of Cu NPs inside and outside the zeolite was 1.2 and 44 nm, respectively, and (2) the amounts of Cu NPs inside the zeolite were constant at ≥0.5 wt %. This calculated S_{total} is shown in Figure S7a. S_{total} was found to increase in proportion to the Cu amounts at <0.5 wt % and be saturated at 0.5 wt %, which is a similar trend to the yield of benzaldehyde (Figure S5a). Additionally, the yield was proportional to S_{total}, as shown in Figure S7b. This indicates that the effective catalytic activities of Cu NPs in pores of zeolite were due to the large surface area, which was realized by the formation of nonaggregating Cu NPs in pores of zeolite.

To expand the substrate scope, we also evaluated the catalytic activity for the aerobic oxidation of various primary alcohols, as shown in Table 2. We selected aromatic alcohols with electron-withdrawing groups (4-nitrobenzyl alcohol) and

Table 2. Catalytic Activity of CuY0.5 for the Aerobic Oxidation of Various Primary Alcohols

$$R - CH_2OH \xrightarrow{CuY0.5} RCHO$$

entries	R	oxidant	reaction temperature (°C)	reaction time (h)	TOF (h^{-1})
1	Ph	air	60	6	17
2	*o*-$MeOC_6H_4$	air	60	6	1.9
3	*m*-$MeOC_6H_4$	air	60	6	19
4	*p*-$MeOC_6H_4$	air	60	6	16
5	*p*-$NO_2C_6H_4$	air	60	24	0.3
6	C_5H_{11}	air	60	24	0.5
7	C_6H_{13}	air	60	24	0.1
8	C_7H_{15}	air	60	24	1.2

electron-donating groups (2-methoxybenzyl alcohol, 3-methoxybenzyl alcohol, 4-methoxybenzyl alcohol) and aliphatic alcohol (1-hexanol, 1-heptanol, 1-octanol) to investigate the interaction between zeolite and the benzene ring. These alcohols were reacted under the same condition as benzyl alcohol for 6 or 24 h using CuY0.5. The TOF values for 3-methoxybenzyl alcohol of 19 h^{-1} and 4-methoxybenzyl alcohol of 16 h^{-1} were comparable to that of the benzyl alcohol, whereas other alcohols hardly reacted. This result indicates that the interaction between zeolite and the benzene ring contributed to this reaction. In the case of aromatic alcohols with a nitro group, the group weakened the interaction by withdrawing electrons from the benzene ring, resulting in low reactivity. On the other hand, the TOF value for 2-methoxybenzyl alcohol was lower than that of benzyl alcohol. This is because the methoxy group close to the hydroxy group prevented the alcohol from contacting Cu NPs in the pores of zeolite. To support the contribution of the interaction to the reaction, we also investigated the catalytic activity for the aerobic oxidation of benzyl alcohol using CuY0.5 and water as a solvent, not acetonitrile. However, the catalytic reaction did not proceed using water as a solvent. In previous reports, water, a polar solvent, weakens the interaction between zeolite and the benzene ring.[47] Therefore, this result supports the contribution of the interaction between the zeolite and benzene ring to the reaction using acetonitrile.

CONCLUSIONS

Nonaggregating Cu NPs were synthesized in the pores of Y-type zeolite by the photoreduction method. EDX analysis and HRTEM images revealed that most of the Cu NPs were uniformly distributed less than 1.2 nm in diameter. XRD patterns and UV−Vis spectra supported the homogeneous distribution of Cu NPs. The catalytic activity was evaluated for the aerobic oxidation of benzyl alcohol. It was found that pore-loaded zeolite had a maximum TOF of 17 h^{-1}. This value is higher than those of any other reports, where Cu NPs and air were used as catalysts and oxidizing agents, respectively. The yield of benzaldehyde increased in proportion to the amount of Cu loading at smaller than 0.5 wt %, indicating that Cu NPs of ≤1.2 nm in pores of zeolite worked as catalysts for benzyl alcohol oxidation. In contrast, the yield was saturated at >0.5 wt %, indicating that large Cu NPs (∼44 nm) were less effective for catalytic reactions. The catalytic reaction for other aromatic alcohols with electron-donating groups proceeded, whereas it did not proceed for the aromatic alcohols with electron-withdrawing groups or aliphatic alcohols, indicating

https://doi.org/10.1021/acsomega.3c07156
ACS Omega 2024, 9, 970−976

that the interaction between zeolite and the benzene ring also contributed to the reaction. From these results, we concluded that nonaggregating Cu NPs of ≤1.2 nm in pores of zeolite brought high catalytic activities. This study would contribute to the development of Cu NP catalysts.

■ ASSOCIATED CONTENT

Supporting Information

The Supporting Information is available free of charge at https://pubs.acs.org/doi/10.1021/acsomega.3c07156.

A listing of the contents of each file supplied as Supporting Information should be included; Leaching test, calculation of absorption cross-section, quantitative analysis of EDX before and after catalytic reaction, and recycling performance; Supporting Figures (Figures S1−S7); Supporting Table (Table S1) (PDF)

■ AUTHOR INFORMATION

Corresponding Author

Hideki Tanaka − *Department of Applied Chemistry, Faculty of Science and Engineering, Chuo University, Tokyo 112-8551, Japan*; orcid.org/0000-0001-7295-1954; Email: htanaka@kc.chuo-u.ac.jp

Authors

Shunya Sakane − *Department of Applied Chemistry, Faculty of Science and Engineering, Chuo University, Tokyo 112-8551, Japan*

Kai Akimoto − *Department of Applied Chemistry, Faculty of Science and Engineering, Chuo University, Tokyo 112-8551, Japan*

Kishin Konishi − *Department of Applied Chemistry, Faculty of Science and Engineering, Chuo University, Tokyo 112-8551, Japan*

Kenta Takaoka − *Department of Applied Chemistry, Faculty of Science and Engineering, Chuo University, Tokyo 112-8551, Japan*

Harunobu Iwatsuki − *Department of Applied Chemistry, Faculty of Science and Engineering, Chuo University, Tokyo 112-8551, Japan*

Mayu Akutsu − *Department of Chemistry, Faculty of Science, Toho University, Funabashi-shi, Chiba 274-8510, Japan*

Toshiki Sugai − *Department of Chemistry, Faculty of Science, Toho University, Funabashi-shi, Chiba 274-8510, Japan*

Complete contact information is available at: https://pubs.acs.org/10.1021/acsomega.3c07156

Notes

The authors declare no competing financial interest.

■ ACKNOWLEDGMENTS

This work was supported by Grant-in-Aid for Early-Career Scientists Grant Number 21K14479 and Grant-in-Aid for Scientific Research (C) Grant Number 19K05187 from JSPS KAKENHI, Japan.

■ REFERENCES

(1) Osterloh, F. E. Inorganic Nanostructures for Photoelectrochemical and Photocatalytic Water Splitting. *Chem. Soc. Rev.* **2013**, *42*, 2294.

(2) Herves, P.; Lorenzo, M. P.; Marzan, L. M. L.; Dzubiella, J.; Lu, Y.; Ballauff, M. Catalysis by Metallic Nanoparticles in Aqueous Solution: Model Reactions. *Chem. Soc. Rev.* **2012**, *41*, 5577−5587, DOI: 10.1039/c2cs35029g.

(3) Li, Y.; Wang, H.; Xie, L.; Liang, Y.; Hong, G.; Dai, H. MoS2 Nanoparticles Grown on Graphene: An Advanced Catalyst for the Hydrogen Evolution Reaction. *J. Am. Chem. Soc.* **2011**, *133*, 7296−7299.

(4) Tong, H.; Ouyang, S.; Bi, Y.; Umezawa, N.; Oshikiri, M.; Ye, J. Nano-Photocatalytic Materials: Possibilities and Challenges. *Adv. Mater.* **2012**, *24*, 229−251.

(5) Zou, X.; Zhang, Y. Noble Metal-Free Hydrogen Evolution Catalysts for Water Splitting. *Chem. Soc. Rev.* **2015**, *44*, 5148.

(6) Yamazoe, S.; Koyasu, K.; Tsukuda, T. Nonscalable Oxidation Catalysis of Gold Clusters. *Acc. Chem. Res.* **2014**, *47*, 816−824.

(7) Ishida, T.; Nagaoka, M.; Akita, T.; Haruta, M. Deposition of Gold Clusters on Porous Coordination Polymers by Solid Grinding and Their Catalytic Activity in Aerobic Oxidation of Alcohols. *Chem. - Eur. J.* **2008**, *14*, 8456−8460, DOI: 10.1002/chem.200800980.

(8) Dhakshinamoorthy, A.; Garcia, H. Catalysis by Metal Nanoparticles Embedded on Metal−Organic Frameworks. *Chem. Soc. Rev.* **2012**, *41*, 5262−5284.

(9) Sanada, T.; Murakami, C.; Marek, K. G.; Iida, K.; Katada, N.; Okumura, K. Fabrication and Catalytic Activity of Thermally Stable Gold Nanoparticles on Ultrastable Y (USY) Zeolites. *Catalysts* **2013**, *3*, 599−613, DOI: 10.3390/catal3030599.

(10) Chen, L. W.; Tong, L.; Nan, H.; Chu, S. Q.; Liang, H. W. Sub-2 nm Ir Nanoclusters Immobilized on Mesoporous Nitrogen-Doped Carbons as Efficient Catalysts for Selective Hydrogenation. *ACS Appl. Nano Mater.* **2019**, *2*, 6546−6553.

(11) Narayanan, R.; El-Sayed, M. A. Catalysis with Transition Metal Nanoparticles in Colloidal Solution: Nanoparticle Shape Dependence and Stability. *J. Phys. Chem. B* **2005**, *109*, 12663−12676.

(12) Gao, C.; Lyu, F.; Yin, Y. Encapsulated Metal Nanoparticles for Catalysis. *Chem. Rev.* **2021**, *121*, 834−881.

(13) Wang, Y.; Arandiyan, H.; Liu, Y.; Liang, Y.; Peng, Y.; Bartlett, S.; Dai, H.; Rostamnia, S.; Li, J. Template-free Scalable Synthesis of Flower-like $Co_{3-x}Mn_xO_4$ Spinel Catalysts for Toluene Oxidation. *ChemCatChem* **2018**, *10*, 3429−3434.

(14) Sadeghi, H. S.; Yaghoobi, M.; Ghasemzadeh, M. A. Synthesis of Pyrido[2,3-*d*:5,6-*d*′]dipyrimidines Using $CuFe_2O_4$/KCC-1/PMA as A Novel and Efficient Nanocatalyst Under Solvent-Free Conditions. *Appl. Organomet. Chem.* **2022**, *36*, No. e67771, DOI: 10.1002/aoc.6771.

(15) Alamgholiloo, H.; Pesyan, N. N.; Mohammadi, R.; Rostamnia, S.; Shokouhimehr, M. Synergistic Advanced Oxidation Process for the Fast Degradation of Ciprofloxacin Antibiotics Using a GO/CuMOF-Magnetic Ternary Nanocomposite. *J. Environ. Chem. Eng.* **2021**, *9*, No. 105486.

(16) Alamgholiloo, H.; Rostamnia, S.; Zhang, K.; Lee, T. H.; Lee, Y. S.; Varma, R. S.; Jang, H. W.; Shokouhimehr, M. Boosting Aerobic Oxidation of Alcohols via Synergistic Effect between TEMPO and a Composite Fe_3O_4/Cu-BDC/GO Nanocatalyst. *ACS Omega* **2020**, *5*, 5182−5191.

(17) Rostamnia, S.; Gholipour, B.; Liu, X.; Wang, Y.; Arandiyan, H. NH_2-Coordinately Immobilized Tris(8-quinolinolato)Iron onto the Silica Coated Magnetite Nanoparticle: Fe_3O_4@SiO_2-FeQ_3 as a Selective Fentonlike Catalyst for Clean Oxidation of Sulfides. *J. Colloid Interface Sci.* **2018**, *511*, 447−455, DOI: 10.1016/j.jcis.2017.10.028.

(18) Haruta, M.; Daté, M. Advances in the Catalysis of Au Nanoparticles. *Appl. Catal., A* **2001**, *222*, 427−437.

(19) Haruta, M. Catalysis of Gold Nanoparticles Deposited on Metal Oxides. *CATTECH* **2002**, *6*, 102−115.

(20) Daniel, M. C.; Astruc, D. Gold Nanoparticles: Assembly, Supramolecular Chemistry, Quantum-Size-Related Properties, and Applications toward Biology, Catalysis, and Nanotechnology. *Chem. Rev.* **2004**, *104*, 293−346.

(21) Guo, S.; Zhang, S.; Sun, S. Tuning Nanoparticle Catalysis for the Oxygen Reduction Reaction. *Angew. Chem., Int. Ed.* **2013**, *52*, 8526−8544.

(22) Nie, Y.; Li, L.; Wei, Z. Recent Advancements in Pt and Pt-free Catalysts for Oxygen Reduction Reaction. *Chem. Soc. Rev.* **2015**, *44*, 2168.
(23) Gawande, M. B.; Goswami, A.; Felpin, F. X.; Asefa, T.; Huang, X.; Silva, R.; Zou, X.; Zboril, R.; Varma, R. S. Cu and Cu-Based Nanoparticles: Synthesis and Applications in Catalysis. *Chem. Rev.* **2016**, *116*, 3722−3811.
(24) Tsuruya, S.; Okamoto, Y.; Kuwada, T. Benzyl Alcohol Oxidation over Y-Type Zeolite Ion-Exchanged with Copper(II) Ion. *J. Ctalysis* **1979**, *56*, 52−64.
(25) Yahiro, H.; Iwamoto, M. Copper Ion-exchanged Zeolite Catalysts in deNO$_x$ Reaction. *Appl. Catal., A* **2001**, *222*, 163−181.
(26) Vanelderen, P.; Vancauwenbergh, J.; Sels, B. F.; Schoonheydt, R. A. Coordination Chemistry and Reactivity of Copper in Zeolites. *Coord. Chem. Rev.* **2013**, *257*, 483−494.
(27) Sun, H.; Liu, C.; Chen, H. Nature of Cu Active Sites in Zeolite-based Catalysts for Selective Catalytic Oxidation of Methane. *Res. Chem. Intermed.* **2019**, *45*, 5849−5861.
(28) Kharchenko, A.; Lebedev, O. I.; Zholobenko, V.; de Waele, V.; Mintova, S. Formation of Copper Nanoparticles in LTL Nanosized Zeolite: Kinetics Study. *J. Phys. Chem. C* **2016**, *120*, 26300−26308, DOI: 10.1021/acs.jpcc.6b08045.
(29) Seidel, A.; Loos, J.; Boddenberg, B. Copper Nanoparticles in Zeolite Y. *J. Mater. Chem.* **1999**, *9*, 2495−2498.
(30) Subramanian, T.; Pitchumani, K. Selective Reduction of Nitroarenes by using Zeolite-Supported Copper Nanoparticles with 2-Propanol as a Sustainable Reducing Agent. *Chem. Catal. Chem.* **2012**, *4*, 1917−1921.
(31) Miyagawa, M.; Usui, M.; Imura, Y.; Kuwahara, S.; Sugai, T.; Tanaka, H. Aqueous Synthesis of Protectant-Free Copper Nanocubes by a Disproportionation Reaction of Cu_2O on Synthetic Saponite. *Chem. Commun.* **2018**, *54*, 8454.
(32) Nishida, N.; Miyashita, A.; Hashimoto, N.; Murayama, H.; Tanaka, H. Regenerative Synthesis of Copper Nanoparticles by Photoirradiation. *Eur. Phys. J. D* **2011**, *63*, 307−310.
(33) Miyagawa, M.; Maeda, T.; Tokuda, R.; Shibusawa, A.; Aoki, T.; Okumura, K.; Tanaka, H. Precious Metal-like Oxide-Free Copper Nanoparticles: High Oxidation Resistance and Geometric Structure. *RSC Adv.* **2016**, *6*, 104560−104565.
(34) Miyagawa, M.; Shibusawa, A.; Maeda, K.; Tashiro, A.; Sugai, T.; Tanaka, H. Diameter-Controlled Cu Nanoparticles on Saponite and Preparation of Film by Using Spontaneous Phase Separation. *RSC Adv.* **2017**, *7*, 41896.
(35) Miyagawa, M.; Ikeyama, Y.; Kotake, H.; Maeda, T.; Tanaka, H. Environmental-Friendly Degradation of Clay-Hybridized Cu Nanoparticles by Carboxylic Acids. *Chem. Phys. Lett.* **2020**, *753*, No. 137615.
(36) Sakane, S.; Miwa, S.; Miura, T.; Munakata, K.; Ishibe, T.; Nakamura, Y.; Tanaka, H. Thermoelectric Properties of PEDOT:PSS Containing Connected Copper Selenide Nanowires Synthesized by Photoreduction Method. *ACS Omega* **2022**, *7*, 32101−32107.
(37) Sakane, S.; Anji, T.; Yamagishi, I.; Kohara, I.; Tanaka, H. Plasmonic Heating of Copper Nanoparticles with Thermoresponsive Polymers. *Chem. Lett.* **2023**, *52*, 582−585.
(38) Lourderaj, U.; Giri, K.; Sathyamurthy, N. Ground and Excited States of the Monomer and Dimer of Certain Carboxylic Acids. *J. Phys. Chem. A* **2006**, *110*, 2709.
(39) Fukushima, T.; Miyazaki, H.; Asano, S. Properties of HSZ Series. *J. TOSOH Res.* **1989**, *33*, 155−166.
(40) Sharma, M.; Das, B.; Sharma, M.; Deka, B. K.; Park, Y. B.; Bhargava, S. K.; Bania, K. K. Pd/Cu-Oxide Nanoconjugate at Zeolite-Y Crystallite Crafting the Mesoporous Channels for Selective Oxidation of Benzyl-Alcohols. *ACS Appl. Mater. Interfaces.* **2017**, *9*, 35453−35462.
(41) Iwamoto, M.; Yokoo, S.; Sakai, K.; Kagawa, S. Catalytic decomposition of nitric oxide over copper(II)-exchanged, Y-type zeolites. *J. Chem. Soc., Faraday Trans. 1* **1981**, *77*, No. 1629, DOI: 10.1039/f19817701629.
(42) Koike, M.; Sakai, R.; Enomoto, S.; Mino, T.; Sugimura, N.; Gotoh, T.; Wada, H.; Shimojima, A.; Kuroda, K. Encapsulation of Cu Nanoparticles in Nanovoids of Plate-like Silica Sodalite through Interlayer Condensation of Cu^{2+} Ion-exchanged Layered Silicate RUB-15. *Dalton Trans.* **2020**, *49*, 8067−8074.
(43) Dutta, D.; Phukan, A.; Dutta, D. K. Nanoporous Montmorillonite Clay Stabilized Copper Nanoparticles: Efficient and Reusable Catalyst for Oxidation of Alcohols. *Mol. Catal.* **2018**, *451*, 148−185, DOI: 10.1016/j.mcat.2017.12.032.
(44) Zhu, Y.; Shen, M.; Xia, Y.; Lu, M. Copper Nanoparticles on Dichromium Trioxide: A Highly Efficient Catalyst from Copper Chromium Hydrotalcite for Oxidant-Free Dehydrogenation of Alcohols. *Appl. Organometal. Chem.* **2015**, *29*, 152−156.
(45) Pande, S.; Saha, A.; Jana, S.; Sarkar, S.; Basu, M.; Pradhan, M.; Sinha, A. K.; Saha, S.; Pal, A.; Pal, T. Resin-Immobilized CuO and Cu Nanocomposites for Alcohol Oxidation. *Org. Lett.* **2008**, *10*, 5179−5181.
(46) Baruah, D.; Saikia, U. P.; Pahari, P.; Konwar, D. Cu-Nanoparticles on Cellulose/H_2O−CH_3CN/Microwave: A Green System for the Selective Oxidation of Alcohols to Aldehydes. *Tetrahedron Lett.* **2015**, *56*, 2543.
(47) Thomas, K. J.; Sunoj, R. B.; Chandrasekhar, J.; Ramamurthy, V. Cation-π-Interaction Promoted Aggregation of Aromatic Molecules and Energy Transfer within Y Zeolites. *Langmuir* **2000**, *16*, 4912−4921, DOI: 10.1021/la991654s.

https://doi.org/10.1021/acsomega.3c07156
ACS Omega 2024, 9, 970−976